CARBON letters

Original Articles
Carbon Letters Vol. 26, 81-87 (2018)

Comparative study on the morphological properties of graphene nanoplatelets prepared by an oxidative and non-oxidative route

Jung-Chul An[1], Eun Jung Lee[1], So-Young Yoon[1], Seong-Young Lee[2] and Yong-Jung Kim[1,♠]

[1]Energy Materials Research Group, Research Institute of Industrial Science & Technology (RIST), Pohang 37673, Korea
[2]Materials Solution Research Group, Research Institute of Industrial Science & Technology (RIST), Pohang 37673, Korea

Article Info

Received 25 October 2017
Accepted 19 December 2017

♠Corresponding Author
E-mail: ykimj@rist.re.kr
Tel: +82-54-279-6713

Open Access

DOI: http://dx.doi.org/10.5714/CL.2018.26.081

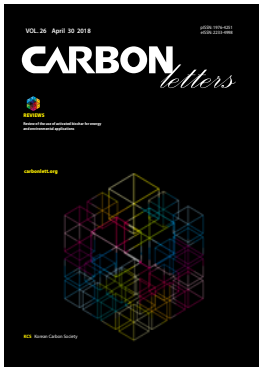

http://carbonlett.org

pISSN: 1976-4251
eISSN: 2233-4998

Abstract

Morphological differences in multi-layered graphene flakes or graphene nanoplatelets prepared by oxidative (rGO-NP, reduced graphene oxide-nanoplatelets) and non-oxidative (GIC-NP, graphite intercalation compound-nanoplatelets) routes were investigated with various analytical methods. Both types of NPs have similar specific surface areas but very different structural differences. Therefore, this study proposes an effective and simple method to identify structural differences in graphene-like allotropes. The adsorptive potential peaks of rGO-NP attained by the density functional theory method were found to be more scattered over the basal and non-basal regions than those of GIC-NP. Raman spectra and high resolution TEM images showed more distinctive crystallographic defects in the rGO-NP than in the GIC-NP. Because the R-ratio values of the edge and basal plane of the sample were maintained and relatively similar in the rGO-NP (0.944 for edge & 1.026 for basal), the discrepancy between those values in the GIC-NP were found to be much greater (0.918 for edge & 0.164 for basal). The electrical conductivity results showed a remarkable gap between the rGO-NP and GIC-NP attributed to their inherent morphological and crystallographic properties.

Key words: graphene nanoplatelets, reduced graphene oxide, graphite intercalation compound, adsorptive potential, density functional theory method

1. Introduction

Graphene has a single-layered graphitic network of carbon atoms with a two-dimensional sp^2-hybrid orbital structure and is generally prepared by either chemical vapor deposition/growth or mechanical exfoliation. A graphene flake or graphene (nano) platelet, however, consists of several layers of graphene and is known to be a more mass production-friendly material because of its relative simplicity of production. A graphene flake is normally produced by delamination of graphite [1-3]. Among the various production techniques to produce graphene flake material, chemical delamination of graphite either via a graphite oxide (GO) [4-9] or graphite intercalation compound (GIC) state [10-13] is the most popular process for its scalability and versatility [14]. Delamination of graphite via the GIC state is known to yield a more chemically pure and a less crystallographically defective graphene flake than product via the GO process because strong oxidants are generally excluded in its preparation process. However, the preparation process via the GIC state is also known to be less effective in the exfoliation of the graphene layers of graphite yielding relatively thicker graphene flakes than that of the GO process.

In this work, two types of graphene flakes produced via the non-oxidative and oxidative route were compared in terms of their morphology, crystallographic order, adsorption poten-

tial of gas and electrical conductivity. The appropriate application field is proposed for the graphene flake which was prepared by a distinguishable chemical preparation route. Evaluation methods introduced in this work can be applied to examine the physical and chemical properties of mass-produced graphene flake products either qualitatively or quantitatively.

2. Experimental

2.1. Materials

Flake natural graphite (Asbury Carbon Co., carbon content >99.9%, average size=250 μm) was used as a starting material for the GIC route of the graphene flakes preparation. Sulfuric acid (Aldrich, assay=99.99%, reagent grade) and hydrogen peroxide solution (Aldrich, 30% [w/w] in H_2O) were used in the GIC formation step as an intercalant and an oxidizing agent, respectively. For a comparative study, commercial reduced graphene oxide (rGO) sample flakes produced by an oxidative route was purchased from a commercial graphene manufacturer (Standard Graphene, rGO-V20-100, carbon content 88%–90%) and used without further treatment.

2.2. Sample preparation

2.2.1. Preparation of the graphene flakes by the non-oxidative method

One gram of flake natural graphite was soaked in 50 mL of hydrogen peroxide solution for 24 h for the partial oxidation. Then, 0.5 g of the graphite-hydrogen peroxide mixture was added to 100 mL of sulfuric acid slowly and stirred overnight to prepare the GIC. After being rinsed with deionized water to remove any extra acid, the GIC was dried for 12 h in a vacuum oven. A commercial-grade microwave oven (LG, MW231GBM, power=800 W) was used to prepare the expanded graphite from the GIC by rapid heating treatment in a short time period (<5 min). The attained expanded graphite specimens were placed in isopropyl alcohol at a concentration of 0.5 wt% and pulverized with an ultrasonic wave generator (wave frequency=40 kHz, power=750 W) for 60 min to prepare the graphene platelets through delamination.

2.3. Characterization

Raman spectra were taken with a 532 nm laser line (XperRam 200, Nanobase). The optical power at the sample was maintained at 5 mW to minimize the thermal shifts of peaks in the Raman spectra as well as the damage to the sample driven by local overheating. The curve fitting was carried out using the Lorentzian distribution function. Averaged R-value (I_D/I_G) from multiple measurements was taken after exclusion of the maximum and minimum values. To compare the R-value at the basal plane and edge of the samples, a focused Raman laser beam was spotted over the center plane region perpendicularly aligned with the beam (as the basal plane part) or perimeter region (as the edge part) of the specimen with the help of an optical microscope. The mean diameter of the products was measured by a particle size analyzer (CILAS, 920). Thus, 0.025 g of the sample were added to 5 mL of isopropyl alcohol, and then dispersed for 30 s. in an ultrasonic bath prior to the measurement. The Brunauer-Emmett-Teller (BET) surface area, density functional theory (DFT) surface area and adsorption potential deconvoluted into the basal, edge and defect surfaces of the sample were determined by standard nitrogen adsorption (77 K) on a Micromeritics ASAP 2020 surface area analyzer. The evaluation of the adsorption data based on the DFT model is embedded in the software from Micromeritics and follows the theory by Ross and Oliver [15]. The crystalline structure of the samples was confirmed by an X-ray diffractometer (Rigaku Dmax2500/PC, Japan) with two goniometer systems. The accelerating voltage and current for a measurement were 40 kV and 200 mA, respectively. Electric conductivity of the products was measured by a 4-point probe type powder resistivity measurement system (HANTech, HPRM-1000) at a pressure range of 5 to 38 MPa. The topographical information of the specimens was attained by a C_s-corrected high resolution tunneling electron microscope (HRTEM, JEOL, JEM-ARM200F) at an accelerating voltage of 80 kV.

3. Results and Discussion

Fig. 1 shows the distributions of the lateral size of the samples measured by the dynamic light scattering analysis method. The average lateral size of the graphene sample prepared by the oxidative method (rGO-NP, reduced graphene oxide-nanoplatelets) was 33.4 μm, while the graphene sample prepared by the non-oxidative method (GIC-NP, graphite intercalation compound-nanoplatelets) had a relatively smaller lateral size at 27.2 μm.

The isotherms of the nitrogen adsorption/desorption plots of the rGO-NP and GIC-NP samples are presented in Fig. 2. The adsorption isotherm of rGO-NP is of type IV, while graphene nanoplatelets-NP can be categorized into type II. Although the specific surface area of both samples fell within a similar value, there was a big difference in the pore structure

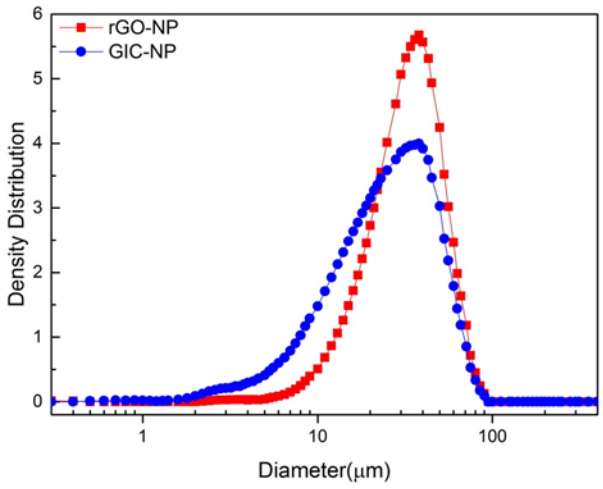

Fig. 1. Lateral size distribution of the graphene materials prepared by oxidative (rGO-NP) and non-oxidative (GIC-NP) methods.

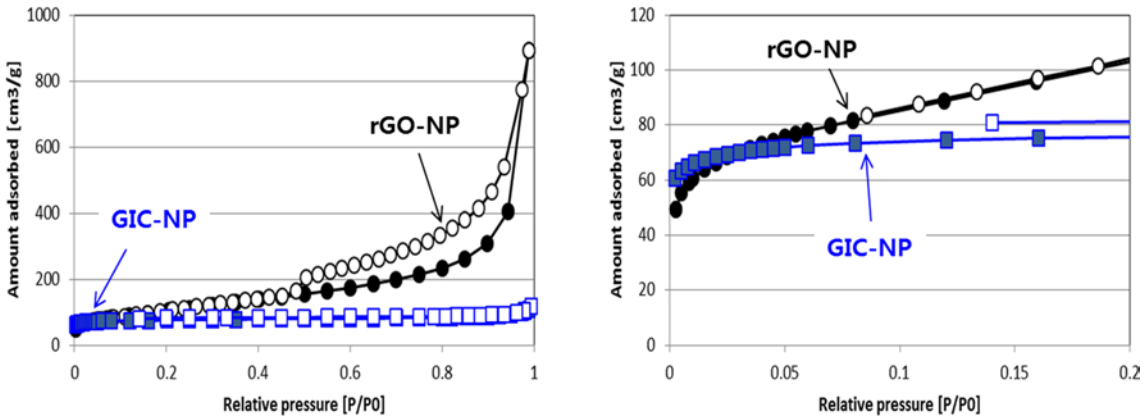

Fig. 2. Isotherms of the nitrogen adsorption/desorption plots of the graphene materials prepared by oxidative (rGO-NP) and non-oxidative (GIC-NP) methods at a relative pressure range of (a) $0<P/P_0<1$ and (b) $0<P/P_0<0.2$.

Table 1. Summary of the nitrogen adsorption properties of the graphene samples prepared by oxidative (rGO-NP) and non-oxidative (GIC-NP) methods

Sample	SSA[a)]	TPV[b)]	V_{BJH}[c)]	APD[d)]	SSA-D[e)]
GIC-NP	301	0.1556	0.0782	2.07	335
rGO-NP	325	0.9485	1.3766	11.67	447

[a)]SSA: specific surface area by BET method ($m^2\ g^{-1}$).
[b)]TPV: total pore volume ($cm^3\ g^{-1}$).
[c)]V_{BJH}: pore volume obtained by BJH method ($cm^3\ g^{-1}$).
[d)]APD: average pore diameter (nm).
[e)]SSA-D: specific surface area by DFT method ($m^2\ g^{-1}$).

including the pore volume, meso-porosity, and average pore diameter. The low bulk density originating from the larger pore volume of the rGO-NP may adversely affect the processability and handling during mass production. Pore properties from the isotherms are summarized in Table 1. Specific surface area, total pore volume at 0.95 in relative pressure (P/P_0), pore volume and average pore diameter were provided. Fig. 3a presents the incremental surface area vs. adsorptive potential plots obtained by the DFT analysis of the rGO-NP and GIC-NP samples. The figure provides information on how nitrogen is adsorbed at different energies depending on the surface of the graphene platelets. Adsorption potentials are generally determined by the density variation of the adsorbent atoms at the interface [15]. The calculation method for adsorption potentials is well described in a previous study [16]. The calculation of the adsorption energy is based on a model for describing adsorption on an energetically heterogeneous surface. However, a realistic adsorption surface has a surface with different affinities for nitrogen atoms corresponding to different adsorption potentials. In the case of physical adsorption, the adsorptive potential is largely determined by the density of the adsorbent constituent atoms at the adsorbing interface. This can be expressed by Eq. 1 as follows:

$$Q(p) = \int q(p,\varepsilon)f(\varepsilon)\, d\varepsilon \quad (1)$$

, where Q(p) is an experimental adsorption isotherm; f(ε) is the adsorptive potential distribution by area, and q(p,ε) is a function describing the theoretical adsorption isotherm on an energetically uniform surface. In this formula, f(ε) implies the adsorptive energy to be confirmed by the DFT method. The adsorptive potential distribution of the rGO-NP was quite broad indicating a diverse surface heterogeneity. The adsorptive potential peaks of the GIC-NP, however, showed a very narrow distribution around 50 K presenting a relative homogeneity in the surface morphology. Previous works [17-19] have shown that the adsorption energy centered around 50–60 K is generally attributed to the basal planes of the graphite. An adsorption energy below 50 K is relevant to the edge/prismatic planes while an energy above 60 K corresponds to a defect of the graphite. From the analysis, rGO-NP was found to possess plenty of heterogeneous and non-basal structures (i.e., edge and defect) on the surface whereas GIC-NP has a homogeneous basal and edge structure. The BET and DFT surface areas of the samples used in this study are summarized in Table 1. The difference in the BET and DFT surface area is generally caused by different assumptions (i.e., a heterogeneous surface for the DFT method vs. a homogeneous surface for the BET method) in the data analysis [16].

Fig. 4 shows the difference in crystallinity between the GIC-NP and rGO-NP. Though there was no big difference in the specific surface area (301 $m^2\ g^{-1}$ for GIP-NP and 325$m^2\ g^{-1}$ for rGO-NP), the crystalline structures of the samples

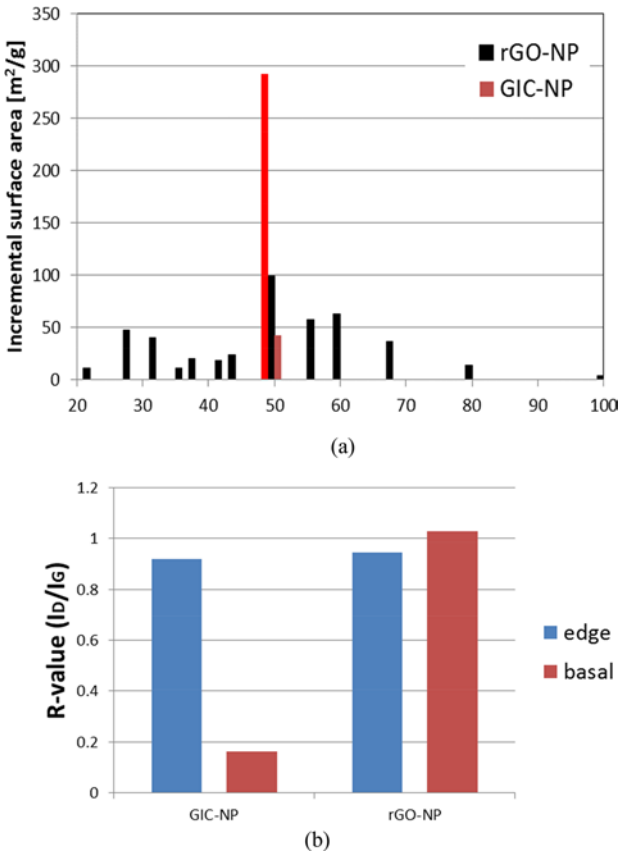

Fig. 3. (a) Incremental surface area vs. adsorptive potential plot of the graphene materials prepared by oxidative (rGO-NP) and non-oxidative (GIC-NP) methods. (b) Plot of the variation in the R-value (I_D/I_G) based on the region (edge or basal) of the graphenes prepared by oxidative (rGO-NP) and non-oxidative (GIC-NP) methods.

were clearly distinguishable. As for the GIP-NP, the crystalline structure inherited from the pristine graphite was clearly confirmed with characteristic graphite diffraction peaks. However, for the rGO-NP, the graphitic crystallinity was barely observed due to its intrinsic defects caused by the harsh acidic reaction condition in the preparation steps. The different preparation route and reaction condition are believed to have caused the significant difference in the crystallinity of the graphene products. Therefore, to characterize the graphene product with better accuracy, the crystallinity of its lattice structure should be carefully examined in addition to its specific surface area. To study the relevance between the type of plane and the defect density, the R-values (I_D/I_G) for both the GIC-NP and rGO-NP were compared. The R-values of the graphene samples were calculated from the relative intensity of the G (ca. 1580 cm^{-1}) and D (ca. 1350 cm^{-1}) peaks [20]. As seen in Table 2 and Fig. 3b, the R-values measured from the edge and basal plane of rGO-NP were very similar with each other indicating an even distribution of the crystallographic defects found on the overall surface of the rGO-NP specimen. Fig. 5e and f show the discrete Raman spectrum for the edge and basal plane of the rGO-NP sample, respectively. The representative deconvoluted plots were made for which the deviation of the R-value was minimized. However, the GIC-NP had a distinctive and diminished R-value on the basal plane implying that a less defective crystallographic structure is found on the basal plane than on the edge plane. The individual Raman spectrum for the edge and basal plane of the GIC-NP sample are shown in Fig. 5c and d, respectively. The degree of discrepancy in the R-values measured from the edge and basal planes of the samples can be an effective indicator distinguishing the production route of the graphene nanoplatelets (e.g., either the oxidative or non-oxidative route). The variation in the crystallographic structure based on the plane type of the graphene platelet samples (i.e., edge vs. basal) was investigated with the Cs-corrected TEM shown in Fig. 6. While the GIC-NP sample showed distinguishable morphologies between the edge and basal planes

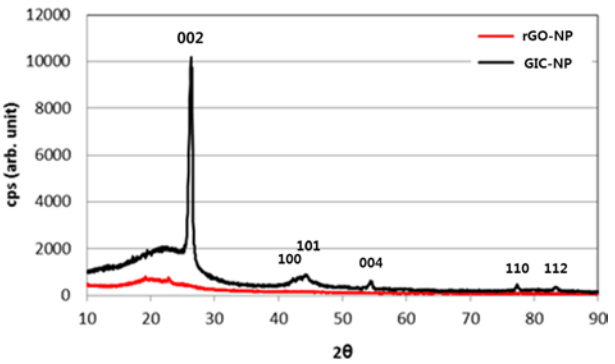

Fig. 4. X-ray diffraction data of the graphene materials prepared by oxidative (rGO-NP) and non-oxidative (GIC-NP) methods.

Table 2. Raman spectroscopy result

Sample	Peak	Raman shift, cm^{-1}	Intensity	R-ratio (I_D/I_G)
Pristine Graphite (edge)	D	1344	0.23×10^6	0.139
	G	1576	1.63×10^6	
Pristine Graphite (basal)	D	1342	0.06×10^6	0.042
	G	1577	1.43×10^6	
GIC-NP (edge)	D	1340	0.54×10^6	0.918
	G	1577	0.59×10^6	
GIC-NP (basal)	D	1348	0.16×10^6	0.164
	G	1579	0.97×10^6	
rGO-NP (edge)	D	1340	0.24×10^6	0.944
	G	1588	0.25×10^6	
rGO-NP (basal)	D	1348	1.05×10^6	1.026
	G	1593	1.03×10^6	

R-values (I_D/I_G) of the pristine graphite and graphene materials prepared by oxidative (rGO-NP) and non-oxidative (GIC-NP) methods are presented and compared for each of the edge and basal regions.

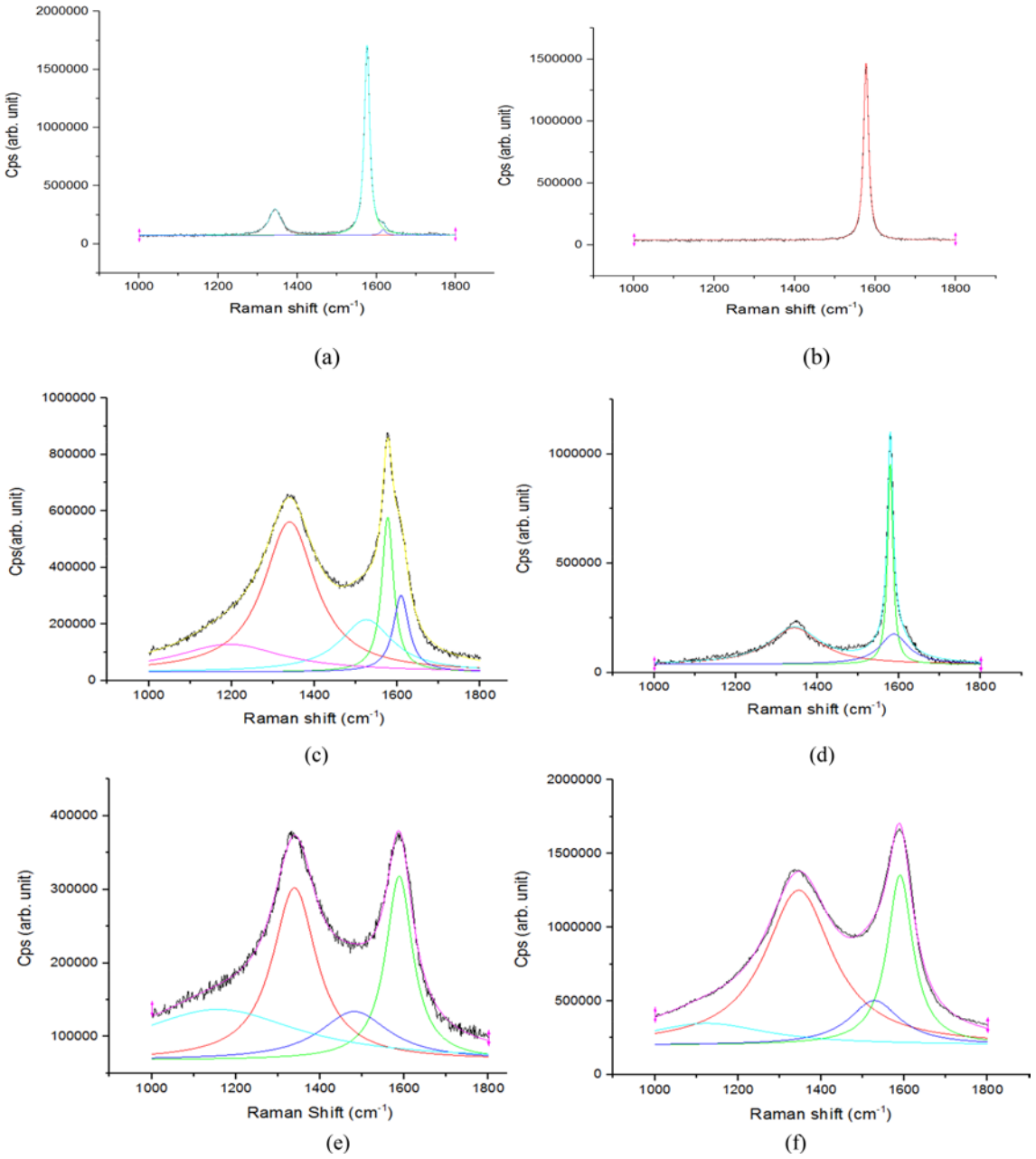

Fig. 5. Raman spectra obtained at the basal and edge region of the samples. (a) Pristine graphite (edge), (b) pristine graphite (basal), (c) GIC-NP (edge), (d) GIC-NP (basal), (e) rGO-NP (edge), (f) rGO-NP (basal). The representative deconvoluted plots were made for which the deviation of the R-value (I_D/I_G) was minimized.

with well-aligned and stacked graphene layers (Fig. 6c) at a certain probing angle, the rGO-NP sample, however, had indistinguishable morphologies between the edge and basal planes implying homogeneous crystallographic structures over the entire observed surface (Fig. 6b). The characteristic morphology difference between the GIC-NP and rGO-NP corresponded to the Raman spectrum shown above. rGO-NP had less dependence on the morphology because the direction of the lattice plane had a universal and indistinguishable crystallographic defect confirmed by the R-values. GIC-NP, however, was found to have a more distinguishable morphology and crystallographic structure which varied based on the type of lattice plane.

The electric conductivities of the rGO-NP and GIC-NP based on the various load cell pressures are shown in Fig. 7. As the compressive pressure was increased, the measured electric conductivity of both samples increased proportionally. Compared to rGO-NP, GIC-NP had a higher electric conductivity in all the experimental conditions. This can be attributed to the lower content of intrinsic defects (i.e., a lower R-value) found in the GIC-

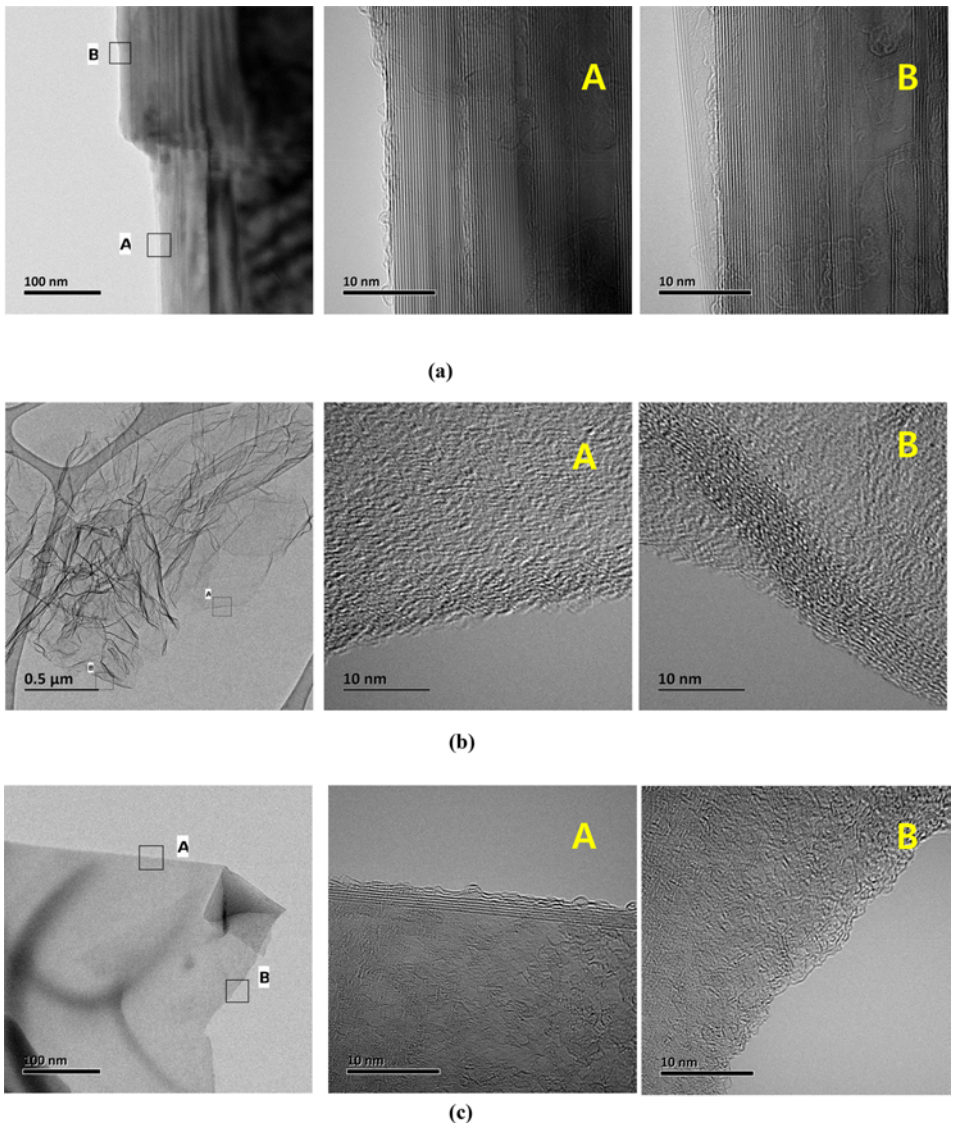

Fig. 6. TEM Photographs of (a) the pristine graphite, (b) the graphene flake via oxidative route (rGO-NP), (c) the graphene flake via non-oxidative route (GIC-NP). The insets in the left images correspond to the magnified images of the right side.

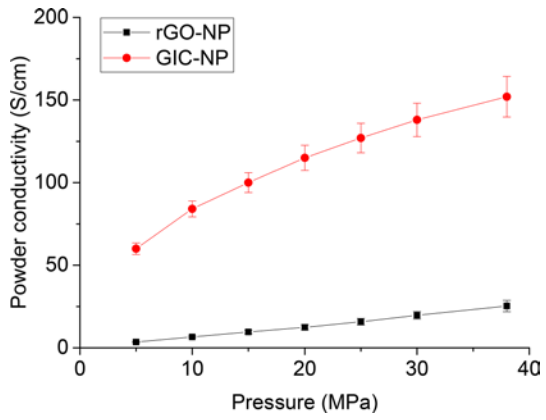

Fig. 7. Powder conductivity of the graphene nanoplatelets prepared by the oxidative route (rGO-NP) and non-oxidative route (GIC-NP).

NP. From this study, the GIC-NP may be regarded as a better candidate for applications such as conductive inks and conductive additives for batteries where the intrinsic electric conductivity is very important.

4. Conclusions

We have compared the morphological differences of graphene nanoplatelets prepared by oxidative (rGO-NP) and non-oxidative (GIC-NP) routes with various analytical methods. The adsorptive potential peaks of the rGO-NP were found to be much more scattered over the basal and non-basal regions than those of the GIC-NP showing a diverse surface heterogeneity. Distinctive crystallographic defects were found in the rGO-NP compared to the GIC-NP as observed by the Raman spectra and TEM images. The R-ratio values measured at the edge and basal

DOI: http://dx.doi.org/10.5714/CL.2018.26.081

plane of the rGO-NP were found to be relatively similar while the GIC-NP showed greater discrepancy between those values. From the overall analytical results and features shown in this comparative study, GIC-NP is believed to be a more favorable material than rGO-NP in various applications such as conductive inks and conductive additives for batteries in which electric conducting properties are very important. Consequently, the degree of discrepancy in the R-values from the edge and basal plane can be used as a critical factor in the quality control of graphite nanoplatelets prepared by various production routes.

Conflict of Interest

No potential conflict of interest relevant to this article was reported.

Acknowledgements

This study was supported by the Graphene Technology Development Program (10044338) funded by the Ministry of Trade, Industry & Energy (MOTIE) of Korea.

References

[1] Zhu L, Zhao X, Li Y, Yu X, Li C, Zhang Q. High-quality production of graphene by liquid-phase exfoliation of expanded graphite. Mater Chem Phys, 137, 984 (2013). https://doi.org/10.1016/j.matchemphys.2012.11.012.

[2] Knieke C, Berger A, Voigt M, Taylor RNK, Röhrl J, Peukert W. Scalable production of graphene sheets by mechanical delamination. Carbon, 48, 3196 (2010). https://doi.org/10.1016/j.carbon.2010.05.003.

[3] Sim HS, Kim TA, Lee KH, Park M. Preparation of graphene nanosheets through repeated supercritical carbon dioxide process. Mater Lett, 89, 343 (2012). https://doi.org/10.1016/j.matlet.2012.08.104.

[4] Park S, Ruoff RS. Synthesis and characterization of chemically modified graphenes. Curr Opin Colloid Interface Sci, 20, 322 (2015). https://doi.org/10.1016/j.cocis.2015.10.006.

[5] Agharkar M, Kochrekar S, Hidouri S, Azeez MA. Trends in green reduction of graphene oxides, issues and challenges: a review. Mater Res Bull, 59, 323 (2014). https://doi.org/10.1016/j.materresbull.2014.07.051.

[6] Krishna R, Fernandes DM, Venkataramana E, Dias C, Ventura J, Freire C, Titus E. Improved reduction of graphene oxide. Mater Today Proc, 2, 423 (2015). https://doi.org/10.1016/j.matpr.2015.04.049.

[7] Gao W, Alemany LB, Ci L, Ajayan PM. New insights into the structure and reduction of graphite oxide. Nat Chem, 1, 403 (2009). https://doi.org/10.1038/nchem.281.

[8] Park S, An J, Potts JR, Velamakanni A, Murali S, Ruoff RS. Hydrazine-reduction of graphite- and graphene oxide. Carbon, 49, 3019 (2011). https://doi.org/10.1016/j.carbon.2011.02.071.

[9] Stankovich S, Dikin DA, Dommett GHB, Kohlhaas KM, Zimney EJ, Stach EA, Piner RD, Nguyen ST, Ruoff RS. Graphene-based composite materials. Nature, 442, 282 (2006). https://doi.org/10.1038/nature04969.

[10] Kalaitzidou K, Fukushima H, Drzal LT. Multifunctional polypropylene composites produced by incorporation of exfoliated graphite nanoplatelets. Carbon, 45, 1446 (2007). https://doi.org/10.1016/j.carbon.2007.03.029.

[11] An JC, Kim HJ, Hong I. Preparation of Kish graphite-based graphene nanoplatelets by GIC (graphite intercalation compound) via process. J Ind Eng Chem, 26, 55 (2015). https://doi.org/10.1016/j.jiec.2014.12.016.

[12] An JC, Lee EJ, Kim BJ, Kim HJ, Kim YJ, Shim J, Hong I. Characterization of graphene nanoplatelets prepared from polyimide-derived graphite. Mater Lett, 161, 321 (2015). https://doi.org/10.1016/j.matlet.2015.08.120.

[13] An JC, Lee EJ, Hong I. Preparation of the spheroidized graphite-derived multi-layered graphene via GIC (graphite intercalation compound) method. J Ind Eng Chem, 47, 56 (2017). https://doi.org/10.1016/j.jiec.2016.12.017.

[14] Park S, Ruoff RS. Chemical methods for the production of graphenes. Nat Nanotechnology, 4, 217 (2009). https://doi.org/10.1038/nnano.2009.58.

[15] Olivier JP, Winter M. Determination of the absolute and relative extents of basal plane surface area and “non-basal plane surface” area of graphites and their impact on anode performance in lithium ion batteries. J Power Sources, 97-98, 151 (2001). https://doi.org/10.1016/s0378-7753(01)00527-4.

[16] Placke T, Siozios V, Schmitz R, Lux SF, Bieker P, Colle C, Meyer HW, Passerini S, Winter M. Influence of graphite surface modifications on the ratio of basal plane to “non-basal plane” surface area and on the anode performance in lithium ion batteries. J Power Sources, 200, 83 (2012). https://doi.org/10.1016/j.jpowsour.2011.10.085.

[17] Foss CEL, Svensson AM, Sunde S, Vullum-Bruer F. Edge/basal/defect ratios in graphite and their influence on the thermal stability of lithium ion batteries. J Power Sources, 317, 177 (2016). https://doi.org/10.1016/j.jpowsour.2016.03.079.

[18] De Volder MFL, Tawfick SH, Baughman RH, Hart AJ. Carbon nanotubes: present and future commercial applications. Science, 339, 535 (2013). https://doi.org/10.1126/science.1222453.

[19] Allen MJ, Tung VC, Kaner RB. Honeycomb carbon: a review of graphene. Chem Rev, 110, 132 (2010). https://doi.org/10.1021/cr900070d.

[20] Zhang L, Aboagye A, Kelkar A, Lai C, Fong H. A review: carbon nanofibers from electrospun polyacrylonitrile and their applications. J Mater Sci, 49, 463 (2014). https://doi.org/10.1007/s10853-013-7705-y.